

From few- to many-body quantum systems

Mauro Schiulaz, Marco Távora, and Lea F. Santos¹

¹*Department of Physics, Yeshiva University, New York, New York 10016, USA*

(Dated: February 12, 2019)

How many particles are necessary to make a many-body quantum system? To answer this question, we take as reference for the many-body limit a quantum system at half-filling and compare its properties with those of a system with N particles, gradually increasing N from 1. We show that the convergence of the static properties of the system with few particles to the many-body limit is fast. For $N \gtrsim 4$, the density of states is already very close to Gaussian and signatures of many-body quantum chaos, such as level repulsion and fully extended eigenstates, become evident. The dynamics, on the other hand, depend on the initial state and time scale. In dilute systems, as the particles move away from each other, the entropy growth changes from linear to logarithmic.

I. INTRODUCTION

Sorites paradoxes are usually illustrated by our inability to precise how many grains of sand constitutes a heap. One grain is not enough, nor two or three grains. But there is a point, even though not well marked, above which the collection of grains can be called a heap. The same question may be extended to the quantum limit: how many particles compose a many-body quantum system? Experiments with cold atoms and trapped ions are promising testbeds for addressing this point. In these experiments, the number of particles can be adjusted as desired [1], which allows for studying how many-body effects emerge as the number of particles increases [2–5]. Rydberg polaritons, where interactions between photons are mediated by atomic Rydberg states, are also a favorable platform for the comparisons between few- and many-body physics [6].

By using a bottom-up approach and increasing one by one the number of ultracold atoms in a quasi-one-dimensional system, it was shown in Ref. [3] that the Fermi sea is formed for $N \geq 4$, where N is the number of atoms. Correspondingly, theoretical studies of thermalization in isolated systems have indicated that the Fermi-Dirac distribution can be obtained also for as few as 4 Fermi particles [7, 8], provided the interactions be sufficiently strong.

In this work, we consider a one-dimensional (1D) spin-1/2 model with short-range interactions, where the number N of spin excitations is conserved. In order for our model to be as generic as possible, we ensure that no local symmetries are present, with the exception of the conservation of the total number of excitations. The case in which half of the chain is filled with excitations is taken as our reference for the many-body limit. In particular, we study how signatures of quantum chaos emerge as N increases from 1. We study both static and dynamic properties. We choose spin-1/2 models due to their accessibility to experiments with nuclear magnetic resonance platforms [9], cold atoms [10], and ion traps [11, 12].

We verify that for $N \gtrsim 4$, the static properties of the spin model with different numbers of excitations become comparable and equivalent to those of the half-filling case. The shape of the density of states (DOS) becomes close to Gaussian, as typical of many-body quantum systems with two-body couplings [13], and signatures of quantum chaos, such as the Wigner-Dyson distribution of the spacings between neighboring levels, rigid spectrum [14], and chaotic eigenstates [15] become evident.

Turning to the dynamics, the threshold between few-body and many-body becomes fuzzier. The behavior of the system depends on the time scale and, quite expectedly, on the separation between the excitations. For initial states where the excitations are very close to each other, the initial evolution after a quench is similar to what we find for chaotic many-body quantum systems. The Shannon (information) entropy, for instance, grows linearly in time [16, 17]. Later, as the excitations spread out, the entropy growth slows down. The behavior of the Shannon entropy becomes logarithmic, similarly to what is seen in disordered many-body systems approaching spatial localization [18, 19]. However, the pre-factors of the logarithms in our clean systems are larger than those in disordered models.

Various tools are available for the analysis of the quench dynamics of 1D systems at the two extreme limits, single particle half filling. The case of $N = 1$ is rather trivial, especially in clean models with short-range couplings, as considered here, while generic properties can often be identified when dealing with chaotic many-body quantum systems [20–22]. We believe that further studies of the region between the two extremes should not only improve our understanding of open problems associated with quantum systems of many interacting particles, such as the quantum-classical correspondence [23] and the metal-insulator transition [24], but may also reveal new [25] and counterintuitive features [26, 27].

The remainder of this paper is organized as follows. In Sec. II, we present the Hamiltonian and describe its main features. In Sec. III, we study the DOS of the model and show how it approaches a Gaussian distribution as N increases. In Sec. IV, we investigate the correlations in the spectrum and how features like level repulsion arise. In Sec. V, we study the structure of the eigenstates and compare them to those of full random matrices. In Sec. VI, we analyze the growth of the Shannon entropy in time. Section VII summarizes our results.

II. SYSTEM MODEL

We study 1D spin-1/2 models described by the following Hamiltonian,

$$\begin{aligned}
 H = & J [d_1 S_1^z + d_L S_L^z \\
 & + \sum_{i=1}^{L-1} (S_i^x S_{i+1}^x + S_i^y S_{i+1}^y + \Delta S_i^z S_{i+1}^z) \\
 & + \lambda \sum_{i=1}^{L-2} (S_i^x S_{i+2}^x + S_i^y S_{i+2}^y + \Delta S_i^z S_{i+2}^z)] .
 \end{aligned} \tag{1}$$

In the above, we set $\hbar = 1$. L is the total number of sites, J is a reference energy scale which we set equal to 1, $S^{x,y,z}$ represents the spin 1/2 operators, $Jd_{1,L}$ correspond to the level spacing of small impurities placed at the edges of the chain, Δ is the anisotropy parameter, and λ is the ratio between nearest-neighbors (NN) and next-nearest-neighbors (NNN) couplings. We refer to a spin pointing up in the z -direction as an excitation.

In the presence of many excitations, the spin model above is a paradigmatic example of many-body quantum systems. When $\lambda = 0$ and $\Delta \neq 0$, Hamiltonian (1) represents the XXZ model, which is integrable. We refer to this case as the NN model to distinguish it from the Hamiltonian with $\lambda \neq 0$, which we name NNN model. The latter is no longer integrable. For $\lambda \sim 1$, the NNN model is strongly chaotic. However, signatures of chaos may get concealed if eigenvalues from different subspaces are mixed [28]. To prevent this from happening, we use parameters that break symmetries. The Hamiltonian (1) conserves the total magnetization in the z -direction, $S^z = \sum_{l=1}^L S_l^z$, so our studies focus on an individual S^z subspace. The isotropic point $\Delta = 1$ is not considered to avoid conservation of total spin. Open boundary conditions are used to break translational invariance. The edge impurities, $d_1 \neq d_L \neq 0$, break spatial inversion symmetry and Ising symmetry for the case where $S^z = 0$. Indeed, when $d_1 \neq d_L \neq 0$, no local conservation laws exist in this model, apart from the conservation of energy and total magnetization in the z -direction.

In the following, we denote by E_α and $|\psi_\alpha\rangle$ the eigenvalues and the corresponding eigenstates of the Hamiltonian. The dimension of a S^z subspace with N excitations is given by $D = L!/N!(L-N)!$.

III. DENSITY OF STATES

The first signature of many-body behavior that we investigate is the DOS, defined as

$$\rho(E) \equiv \sum_{\alpha} \delta(E - E_{\alpha}). \tag{2}$$

For a many-body system with few-body interactions only, the DOS is known to be Gaussian [13, 29]. Our system (1) has only two-body interactions. We therefore investigate how the DOS approaches the Gaussian limit, as excitations are added into the system.

As a warm-up, let us study the case $d_{1,L} = \Delta = \lambda = 0$ with closed boundary conditions. This noninteracting integrable Hamiltonian represents the well-known XX model [30], for which we are able to compute the DOS exactly. In the continuum limit $L \rightarrow \infty$, as shown in Appendix A,

$$\rho_{XX}^{(N)}(E) = \frac{1}{2\pi} \int_{-\infty}^{\infty} d\tau e^{iE\tau} \mathcal{J}_0^N(J\tau), \tag{3}$$

where \mathcal{J}_0 is the Bessel function of the first kind. For $N = 1$, this gives trivially

$$\rho_{XX}^{(1)}(E) = \frac{1}{\pi} \frac{1}{\sqrt{J^2 - E^2}}. \tag{4}$$

For $N > 1$, the DOS for the XX model is plotted in Fig. 1 (a)-(d). From left to right, N grows from 2 to 5. As it can be seen, the peak in the middle of the spectrum becomes progressively smoother and the overall shape of the distribution becomes qualitatively similar to a Gaussian for $N \gtrsim 4$.

The approach to the Gaussian shape can be explained in terms of the central limit theorem. The 1D XX model can be mapped to a model of free fermions [30], which makes it suitable for analytical treatment. As a consequence, the total energies of the system are obtained by simply adding the energies of each excitation. The distribution of the sums of these independent excitation energies is analogous to the distribution of independent random variables, which, according to the central limit theorem, tends to a normal distribution for sufficiently large sample sizes.

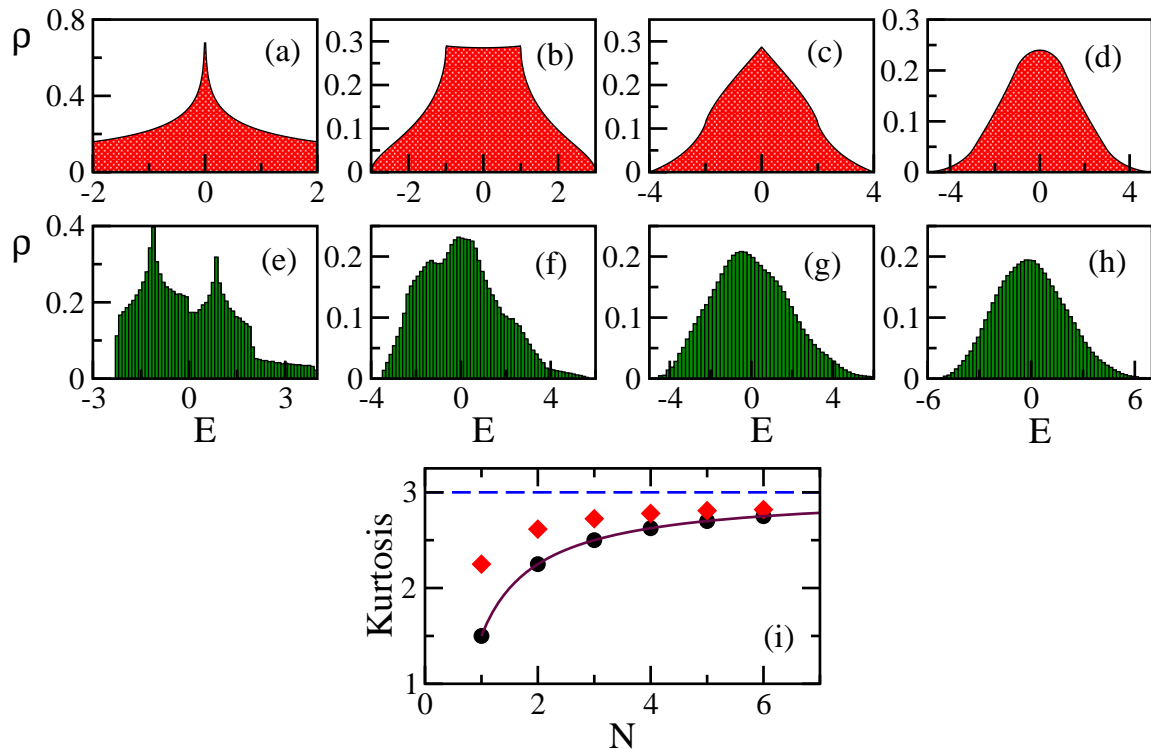


FIG. 1: Density of states for the XX model (a)-(d) and NNN model (e)-(h). From left to right: $N = 2, 3, 4, 5$. For the periodic XX model, we show analytic results in the limit $L \rightarrow \infty$. For the NNN model, we take open boundary conditions and system sizes $L = 200, 50, 28, 21$ from left to right. We choose $\Delta = 0.48$, $\lambda = 1$, $d_1 \simeq 0.05$ and $d_L \simeq 0.09$. The energies are rescaled so that for any L and chosen parameters, the middle of the spectrum is at zero. Panel (i) gives the kurtosis of the DOS as a function of N for the XX (circle) and the NNN (diamond) models. The solid line is the fitting curve for the XX model. The kurtosis approaches 3 as the number of excitations increases.

A more quantitative way to compare the DOS to a Gaussian distribution is to compute the kurtosis,

$$K(N) \equiv \frac{\langle (E - \langle E \rangle)^4 \rangle}{\langle (E - \langle E \rangle)^2 \rangle^2}, \quad (5)$$

where the averages $\langle f(E) \rangle$ are taken on the whole spectrum, weighted by the DOS,

$$\langle f(E) \rangle \equiv \int_{-NJ}^{NJ} dE \rho_{XX}^{(N)}(E) f(E). \quad (6)$$

For a Gaussian distribution, $K_G = 3$. In Appendix A, we show that, for the XX model,

$$K(N) = \frac{\pi \int_{-\infty}^{\infty} d\tau \mathcal{J}_0^N(J\tau) \tau^{-5} [4NJ\tau(N^2J^2\tau^2 - 6) \cos(NJ\tau) + (N^4J^4\tau^4 - 12N^2J^2\tau^2 + 24) \sin(NJ\tau)]}{\left(\int_{-\infty}^{\infty} d\tau \mathcal{J}_0^N(J\tau) \tau^{-3} [2NJ\tau \cos(NJ\tau) + (N^2J^2\tau^2 - 2) \sin(NJ\tau)] \right)^2}. \quad (7)$$

These values of $K(N)$ are plotted in Fig. 1 (i). A power-law fit for these points gives

$$K(N) \sim 3 \left(1 - \frac{1}{2N} \right). \quad (8)$$

This tells us that the spectrum smoothly approaches the many-body limit as N is increased, although there is not a threshold at which the limit is reached.

For the NNN model, no exact results are available, so we resort to numerical simulations. From Fig. 1 (e)-(h), one sees that once again, the shape of the DOS starts looking qualitatively similar to a Gaussian for $N \gtrsim 4$. In each plot, we have shifted the energies by a constant, such that $\langle E \rangle = 0$. Notice that we are numerically limited to relatively small sizes, so the system gets denser for $N \gtrsim 4$. However, the approach to the Gaussian shape is caused by the increased number of excitations and not by the increase of the density, as made clear by the analysis of the XX model in the thermodynamic limit.

The values of the kurtosis for the NNN model are plotted in Fig. 1 (i). They are larger than those obtained for the XX model and they also approach the Gaussian limit, although once again no threshold value at which convergence is achieved can be identified.

IV. ONSET OF CHAOS

One of the most distinctive features of quantum chaos is the strong repulsion between neighboring energy levels. Let us define the spacing

$$s_n \equiv \frac{E_{n+1} - E_n}{Z(E_n)}, \quad (9)$$

where $Z(E_n)$ is a normalization that comes from unfolding the spectrum. [14] Let us take a real symmetric matrix, with entries drawn independently from a Gaussian distribution. A matrix constructed using this procedure is said to belong to the Gaussian Orthogonal Ensemble (GOE) [14, 31]. Using random matrix theory it is possible to show that, for GOE matrices, s is distributed according to the following Wigner-Dyson distribution,

$$P(s) = \frac{\pi s}{2} \exp\left(-\frac{\pi s^2}{4}\right). \quad (10)$$

The most important feature of the Wigner-Dyson distribution is that it vanishes linearly for $s \rightarrow 0$, meaning that the probability of two eigenvalues crossing each other is suppressed. This behavior is due to the fact that the eigenvalues are strongly correlated. The spectra of realistic chaotic systems with real and symmetric Hamiltonian matrices also follow the above Wigner-Dyson distribution

For sequences of uncorrelated eigenvalues, the distribution of s is Poissonian, $P(s) = \exp(-s)$. The eigenvalues of integrable systems often follow this distribution, because they typically display an extensive set of local conserved quantities, which partition the Hilbert space in many uncorrelated sectors. We note, however, that in integrable systems with a large number of degenerate levels or with spectra of the ‘‘picket-fence’’ type, where the eigenvalues are approximately equally spaced, other distributions are found.

In Fig. 2 (a)-(d), we plot the distribution of level spacing for the NNN model, for systems with $N = 2, 3, 4, 5$ excitations. In each plot, we show for comparison the Poisson (red line) and Wigner-Dyson (blue lines) distributions. For $N = 2$, the distribution is intermediate between Poisson and Wigner-Dyson with a visible dip at small s , signaling that some amount of level repulsion is already present in the system. As N is increased, level repulsion becomes more important, and at $N = 4$ the qualitative shape is very close to a Wigner-Dyson distribution.

A way to quantify the transition from Poisson to the Wigner-Dyson distribution is by employing a distribution that interpolates between the two, such as the Brody distribution [13],

$$P_\beta(s) \equiv (\beta + 1)bs^\beta \exp(-bs^{\beta+1}), \quad b \equiv \left[\Gamma\left(\frac{\beta + 2}{\beta + 1}\right)\right]^{\beta+1}, \quad (11)$$

where Γ is Euler’s gamma function. The Poisson distribution corresponds to the case $\beta = 0$, while the Wigner-Dyson distribution to $\beta = 1$. To evaluate quantitatively the effect of level repulsion, we fit our numerical distribution with $P_\beta(s)$ using β as a fitting parameter. The resulting values of β are plotted as a function of N in Fig. 2. As it can be seen, already at $N = 4$ we have $\beta \sim 1$, meaning that indeed a system with 4 excitations can be meaningfully described as chaotic.

Another manifestation of the correlation among energy levels is the rigidity of the spectrum, which can be evaluated with quantities such as the so-called rigidity or the level number variance. Here, we consider the latter, which is obtained as follows. We partition the spectrum in energy intervals of length ℓ and compute the number of eigenvalues inside each interval. The variance of the resulting distribution is the level number variance $\Sigma^2(\ell)$. For full random matrices from the GOE, we have [14]

$$\Sigma^2(\ell) = \frac{2}{\pi^2} \left(\ln(2\pi\ell) + \gamma_e + 1 - \frac{\pi^2}{8} \right), \quad (12)$$

where $\gamma_e = 0.5772\dots$ is Euler’s constant. In contrast, for systems with an uncorrelated spectrum, one finds $\Sigma^2(\ell) = \ell$, while for the harmonic oscillator, one has $\Sigma^2(\ell) = 0$, due to the complete rigidity of the spectrum. $P(s)$ and $\Sigma^2(\ell)$ are complementary. The former characterizes the short-range fluctuations of the spectrum and the latter characterizes the long-range fluctuations.

In Fig. 2 (e)-(h), we plot the function $\Sigma^2(\ell)$ for the NNN model for $N = 2, 3, 4, 5$ excitations. The data (black dots) are compared with the curve for the GOE (red line) and the Poissonian distribution (blue line). For $N = 2$, the data are close to the curve for uncorrelated eigenvalues. $N = 3$ looks intermediate. For $N \gtrsim 4$, the data at different number of excitations do not

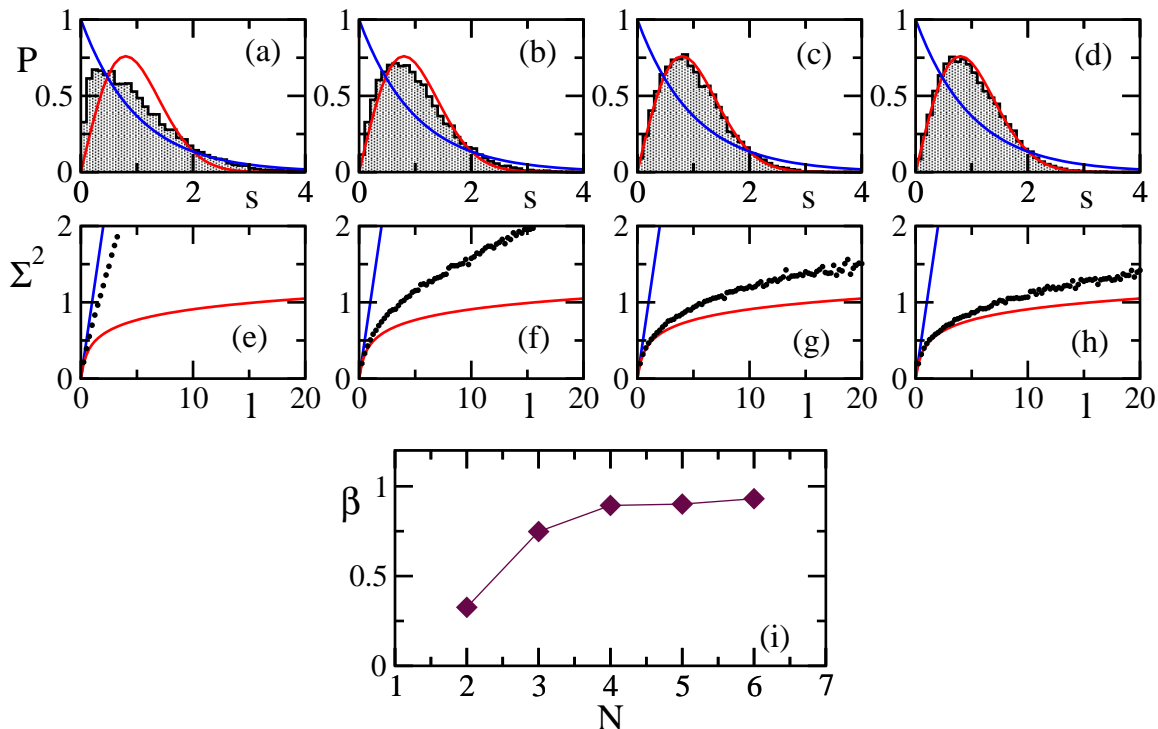


FIG. 2: Level spacing distribution (a)-(d) and level number variance (e)-(h) for the NNN model. From left to right, the system sizes are $L = 200, 50, 28, 21$, respectively, and the numbers of excitations are $N = 2, 3, 4, 5$. Parameters: $\Delta = 0.48$, $\lambda = 1$, $d_1 \simeq 0.05$ and $d_L \simeq 0.09$. Open boundary conditions are taken. In (a)-(d), the grey histogram represents the actual numerical data, which are compared with the Poissonian (blue line) and Wigner-Dyson (red line) distributions. In (e)-(h): numerical data are black dots. They are compared with the result for uncorrelated eigenvalues (blue straight line) and the GOE curve (red logarithmic curve). In (i): the parameter β as a function of N . It converges to the Wigner-Dyson value $\beta = 1$ for $N \gtrsim 4$.

look qualitatively different, which shows that the system acquires a many-body character. It must be noticed that the data follow the GOE curve for small l only. This happens because the spectra of realistic chaotic many-body quantum systems are never as rigid as the spectra of full random matrices, where all degrees of freedom interact with each other. Not all features of a realistic many-body system can be captured by such simple random matrix model.

V. EIGENSTATES

The onset of quantum chaos is reflected also in the structure of the eigenstates. In contrast with the eigenvalues, the study of the eigenstates requires a choice of basis. This choice depends on the physical problem one is interested in. For example, in studies of spatial localization, we employ the site-basis (also known as computational basis), where on each site the spin either points up or down in the z -direction. In the context of quantum chaos, one resorts to the mean-field basis, which corresponds to the eigenstates of the regular (integrable) part of the total Hamiltonian. The perturbation, that breaks integrability and brings the system into the chaotic domain, also couples the mean-field basis vectors. The level of complexity of the eigenstates of the total Hamiltonian depends on the strength of this perturbation.

In the case of the NNN model, we write the eigenstates $|\psi_\alpha\rangle = \sum_n C_n^\alpha |\phi_n\rangle$ in terms of the eigenstates $|\phi_n\rangle$ of the NN model, whose eigenvalues are denoted by ε_n . The distribution

$$R^{(\alpha)}(E) = \sum_n |C_n^\alpha|^2 \delta(E - \varepsilon_n) \quad (13)$$

characterizes the spreading of the eigenstate $|\psi_\alpha\rangle$ in the mean-field basis. In the many-body limit, the shape of $R^{(\alpha)}(E)$ for states away from the borders of the spectrum broadens from nearly a delta function, when $\lambda \sim 0$, to a Gaussian at strong chaos ($\lambda \sim 1$) [17]. In strongly chaotic eigenstates, the coefficients C_n^α are approximately random variables following the Gaussian envelope of the system energy shell. This is equivalent to what happens to the local density of states [16, 17, 32, 33]. The Gaussian shape of $R(E)$ and of the local density of states is a consequence of the Gaussian form of the DOS.

In realistic systems with few-body interactions, only the coefficients C_n^α within the energy shell can be non-zero. This is in contrast with the eigenstates of full random matrices, where all C_n^α are non-zero. The eigenstates of full random matrices are random vectors and therefore fully delocalized in the Hilbert space. One can measure the level of delocalization of the states with quantities such as the participation ratio, defined as

$$PR^{(\alpha)} \equiv \frac{1}{\sum_n |C_n^\alpha|^4}. \quad (14)$$

For full random matrices from GOE, $PR \simeq D/3$ for any eigenstate. In realistic many-body systems, strongly chaotic states also lead to $PR^{(\alpha)} \propto D$, but the pre-factor is smaller than $1/3$.

In Fig. 3 (a)-(d), we plot the function $R^{(\alpha)}(E)$ for an eigenstate $|\psi_\alpha\rangle$ near the middle of the spectrum of the NNN model with $\lambda = 1$. Instead of the dependence on the strength of the perturbation, our goal now is to analyze how the structure of the eigenstates depends on the number of excitations. For $N = 2$, the distribution is sparse, indicating that the eigenstates are far from being fully extended in the energy shell. The level of delocalization increases with N . For $N \gtrsim 4$ the distribution already resembles a Gaussian (red lines), indicating the proximity to the chaotic many-body limit.

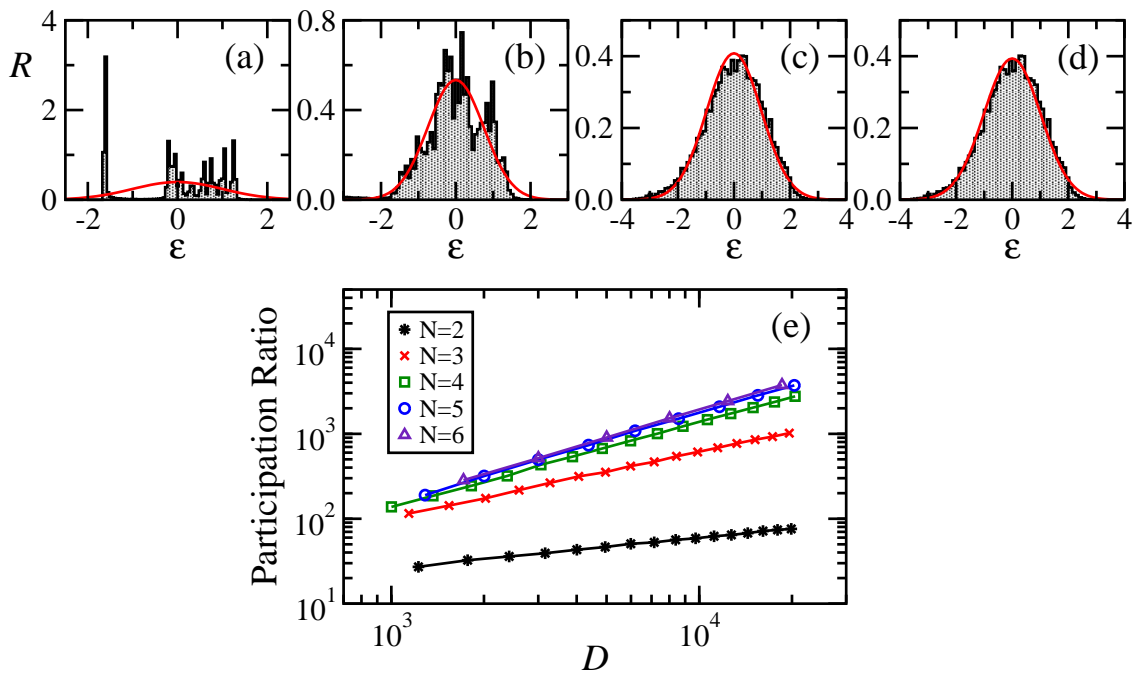


FIG. 3: Energy distribution $R^{(\alpha)}(E)$ of an eigenstate $|\psi_\alpha\rangle$ in the middle of the spectrum of the NNN model (a)-(d) and scaling analysis of the participation ratio for eigenstates written in the mean-field-basis (e). Parameters: $\Delta = 0.48$, $\lambda = 1$, $d_1 \simeq 0.05$ and $d_L \simeq 0.09$. Open boundary conditions are taken. From (a) to (d), the numbers of excitations are $N = 2, 3, 4, 5$. The distributions are shifted, such that $\sum_n |C_n^\alpha|^2 \epsilon_n = 0$, and they are compared with Gaussians (red line) of variance $\sum_n |C_n^\alpha|^2 \epsilon_n^2$. In (e), the data are averaged over 10% of the eigenstates in the middle of the spectrum. Each curve corresponds to a different N (indicated). For $N \gtrsim 4$, $PR \propto D$.

To make a more quantitative analysis, in Fig. 3 (e), we show the scaling of PR as a function of the dimension D for different N 's. For $N < 4$, the scaling is sub-linear, implying that one cannot consider systems with such small number of excitations as fully chaotic. Conversely, for $N \gtrsim 4$, the curves fall closely on top of each other, indicating that the eigenstates have already reached the maximal allowed level of spreading over the mean-field basis for the given perturbation strength.

Unlike the DOS, which approaches the many-body limit smoothly as N is increased, the threshold for PR seems better marked. Its convergence to the many-body limit is clear for $N \gtrsim 4$.

VI. DYNAMICS

All quantities studied up to now are of static nature. In this section, we analyze the real time evolution of the NNN model with $\lambda = 1$. In our simulations, we initialize the system in the following two site-basis states,

$$|\Psi_1^{(N)}(0)\rangle = |\downarrow_1 \cdots \underbrace{\uparrow_j \uparrow_{j+1} \cdots \uparrow_{j+N-2} \uparrow_{j+N-1}}_{N \text{ sites, } N \text{ up-spins}} \cdots \downarrow_L\rangle,$$

$$|\Psi_2^{(N)}(0)\rangle = |\downarrow_1 \cdots \underbrace{\uparrow_j \downarrow_{j+1} \cdots \uparrow_{j+2N-2} \downarrow_{j+2N-1}}_{2N \text{ sites, } N \text{ up-spins}} \cdots \downarrow_L\rangle.$$

In the half filling limit, $|\Psi_1^{(L/2)}(0)\rangle$ coincides with the domain wall state and $|\Psi_2^{(L/2)}(0)\rangle$ with the Néel state state. These states are accessible experimentally [34, 35] and have been extensively investigated in theoretical studies of quench dynamics in the $S^z=0$ subspace.

The quantity chosen for the analysis of the dynamics is the Shannon entropy,

$$S_h(t) \equiv - \sum_j |W_j(t)|^2 \ln |W_j(t)|^2 \quad (15)$$

where $W_j(t) = |\langle \phi_j | e^{-iHt} | \Psi(0) \rangle|^2$. This quantity measures how the initial state spreads into other site-basis vectors $|\phi\rangle$ and it is related to the entanglement entropy [36].

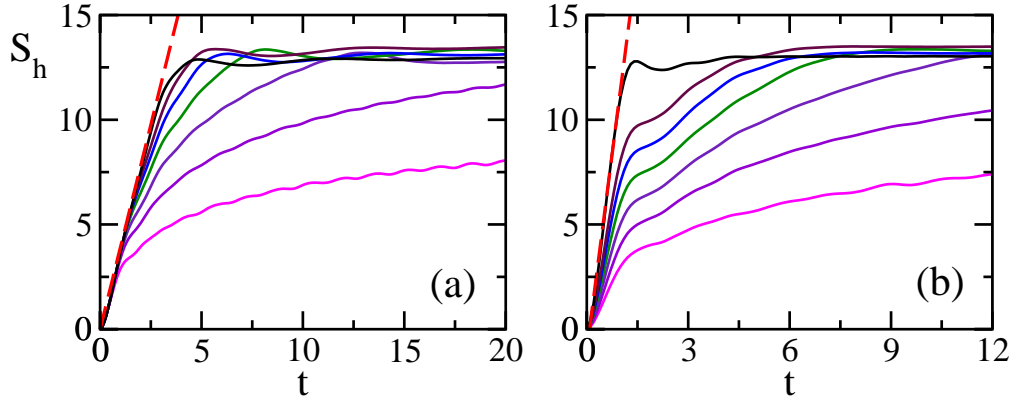


FIG. 4: Evolution of the Shannon entropy in the site-basis. NNN model with $\Delta = 0.5$, $\lambda = 1$, periodic boundary conditions, and no impurities. $|\Psi_1^{(N)}(0)\rangle$ (which becomes the domain wall state at half-filling) is considered in (a) and $|\Psi_2^{(N)}(0)\rangle$ (which becomes the Néel state at half-filling) is used in (b). From bottom to top, the lines correspond to $(L, N) = (1400, 2), (184, 3), (72, 4), (44, 5), (32, 6), (28, 7)$, and $(22, 11)$ (half filling limit). A linear increase (red dashed line) is shown for comparison with the half filled case.

Figure 4 shows the evolution of $S_h(t)$ for $N = 2, 3, 4, 5, 6, 7$ and also for the half-filling limit $N = L/2$. The system sizes used lead to dimensions D of the Hilbert space that are similar for all N 's, so that the saturation of the dynamics for all curves are of the same order. Data for the initial state $|\Psi_1^{(N)}(0)\rangle$ are shown in Fig. 4 (a) and those for $|\Psi_2^{(N)}(0)\rangle$ in Fig. 4 (b).

As expected, for the state $|\Psi_1^{(N)}(0)\rangle$, $S_h(t)$ follows exactly the half-filling curve up to a time scale dependent on N . This happens because the short-time dynamics is restricted to the interface between the up and down spins at the edges of the domain wall. For the state $|\Psi_2^{(N)}(0)\rangle$, the evolution does not follow the half-filling curve at any time.

In the half-filled case, the two initial states qualitatively evolve in the same way. The Shannon entropy grows linearly, indicating that the site-basis vectors are populated exponentially fast in time, as typical of chaotic systems [16, 17, 36]. For the other N 's, the picture is quite different. The linear growth holds for a certain time interval, but then the evolution slows down and becomes logarithmic. The time interval of the linear behavior increases with N , but the crossover between the fast relaxation at short times and the slow dynamics at long times is always visible. This may be interpreted as a crossover from a short-time regime, in which the excitations interact with each other, and a later-time regime, in which the particles are too diluted to experience strong interactions.

We note that a similar change in the dynamical behavior occurs also in many-body models with onsite disorder, as they approach localization in space [18, 19]. However, the pre-factor of the logarithmic behavior in this case is smaller than 1 and related with the fractal dimension of the eigenstates [19]. The pre-factor in our clean model with few excitations is larger than 2 and it increases with N .

The dynamics of the Shannon entropy does not allow us to identify a precise point for the transition from the few- to the many-body behavior. We find only a slow crossover. Nonetheless, the results display interesting features that will be studied in greater detail in a future work. This includes the pre-factor of the logarithmic behavior and how it depends on the number of excitations, the initial states, and the bounds in the energy spectrum [37, 38].

VII. CONCLUSION

While many tools exist to study systems in the single-particle and in the many-body limit, the crossover between these two regimes is still poorly understood. In this work, we analyzed one of the aspects of this crossover, namely how signatures of quantum chaos emerge as the number of excitations increases. We showed that many-body properties associated with the eigenvalues and eigenstates manifest themselves already for as few as $N \gtrsim 4$, although a well defined transition point cannot be identified.

From the point of view of the dynamics of the system, the behavior depends on the time scale. If one initially confines all excitations to a small region, the evolution at short times is dominated by the interactions and the behavior is similar to the many-body case. At long times, the excitations spread out and the effects of the interactions fade away. The analysis of the crossover between the two different temporal regimes is within reach of existing experiments with cold atoms and ion traps, where the number of particles considered in the dynamics can be manipulated.

It is our hope that this work will motivate further research on how the properties of quantum systems change as the number of particles increases. It would be interesting to extend our studies to non-chaotic systems, such as exactly integrable models and many-body localized systems. For the former, analytical results could be obtained, which would serve as reference for further studies. For the latter, one may consider how the localization properties change from few particles to the many-body limit. In particular, a better understanding of how the many-body character of the system is developed might help clarifying the influence of finite size effects on the localization transition [39, 40].

Acknowledgments

This work was funded by the American National Science Foundation (NSF) Grant No. DMR-1603418.

Appendix A: Analytical derivation of the DOS and kurtosis for the XX model

Following Refs. [41–43], we compute the DOS for the XX model with periodic boundary conditions using the coordinate Bethe Ansatz method. We recall that the Hamiltonian of the XX model is

$$H = J \sum_{l=1}^L (S_l^x S_{l+1}^x + S_l^y S_{l+1}^y). \quad (\text{A1})$$

The DOS is defined as

$$\rho_{XX}(E) \equiv \frac{1}{D} \sum_{\alpha=1}^D \delta(E - E_{\alpha}) = \frac{1}{D} \sum_{\alpha=1}^D \int_{-\infty}^{+\infty} \frac{d\tau}{2\pi} e^{i\tau(E - E_{\alpha})}. \quad (\text{A2})$$

1. One excitation

Since the total magnetization of the system is conserved, let us consider first the case $N = 1$, that is, only one spin pointing up in the positive z -direction. We write the eigenstates $|\psi_{\alpha}\rangle$ in the following form,

$$|\psi_{\alpha}\rangle = \sum_{l=1}^L a_l^{\alpha} |\phi_l\rangle, \quad (\text{A3})$$

where $|\phi_l\rangle$ denotes the states of the site-basis (computational-basis),

$$\begin{aligned} |\phi_1\rangle &= |\uparrow\downarrow\downarrow \cdots \downarrow\rangle \\ |\phi_2\rangle &= |\downarrow\uparrow\downarrow \cdots \downarrow\rangle \\ &\dots \end{aligned} \quad (\text{A4})$$

To find the coefficients a_l^α , we solve the Schrödinger equation

$$H |\psi_\alpha\rangle = E_\alpha |\psi_\alpha\rangle, \quad (\text{A5})$$

where E_α is the eigenenergy of state $|\psi_\alpha\rangle$. The Hamiltonian acts on the states $|\phi_l\rangle$ as follows,

$$\begin{aligned} H |\phi_1\rangle &= \frac{J}{2} (|\phi_L\rangle + |\phi_2\rangle); \\ H |\phi_l\rangle &= \frac{J}{2} (|\phi_{l-1}\rangle + |\phi_{l+1}\rangle), \quad l \neq 1, L; \\ H |\phi_L\rangle &= \frac{J}{2} (|\phi_{L-1}\rangle + |\phi_L\rangle). \end{aligned} \quad (\text{A6})$$

Substituting these relations into Eq. (A5) and collecting terms with the same index l , we get the equation

$$E_\alpha a_l^\alpha = \frac{J}{2} (a_{l-1}^\alpha + a_{l+1}^\alpha). \quad (\text{A7})$$

We now make the following Ansatz for the coefficients a_l^α ,

$$a_l^\alpha = e^{i\theta l}, \quad (\text{A8})$$

where θ is a real number yet to be determined. Substituting into Eq. (A7), we find that

$$E_\alpha = J \cos \theta. \quad (\text{A9})$$

We now invoke the periodic boundary conditions. Since

$$a_{l+L} = a_l, \quad (\text{A10})$$

we have that

$$\theta = \frac{2\pi k}{L}, \quad (\text{A11})$$

with $k \in \{0, \pm 1, \pm 2, \dots, \pm (\frac{L}{2} - 1), \frac{L}{2}\}$.

In hands of the eigenvalues, we can obtain the DOS,

$$\rho_{XX}^{(1)}(E) = \frac{1}{L} \sum_k \int_{-\infty}^{+\infty} \frac{d\tau}{2\pi} e^{i\tau[E - J \cos(\frac{2\pi k}{L})]}. \quad (\text{A12})$$

For $L \gg 1$, we can take the continuum limit, making the substitution

$$\frac{1}{L} \sum_k \rightarrow \int_{-\pi}^{\pi} \frac{dq}{2\pi}. \quad (\text{A13})$$

This yields

$$\rho_{XX}^{(1)}(E) = \int_{-\pi}^{\pi} \frac{dq}{2\pi} \int_{-\infty}^{+\infty} \frac{d\tau}{2\pi} e^{i\tau(E - J \cos q)} = \int_{-\infty}^{+\infty} \frac{d\tau}{2\pi} e^{iE\tau} \mathcal{J}_0(J\tau) = \frac{1}{\pi\sqrt{J^2 - E^2}}. \quad (\text{A14})$$

In the above, \mathcal{J}_0 is the Bessel function of the first kind.

2. Two excitations and generic N

This treatment can be extended to generic values of N . The eigenstates can be written as

$$|\psi_\alpha\rangle = \sum_{l_1, l_2, \dots, l_N=1}^L a_{l_1, l_2, \dots, l_N}^\alpha |\phi_{l_1, l_2, \dots, l_N}\rangle, \quad (\text{A15})$$

and the eigenvalues turn out to be

$$E_\alpha = J \sum_{i=1}^N \cos\left(\frac{2\pi k_i}{L}\right), \quad (\text{A16})$$

with $k_1 < k_2 < \dots < k_N$. Let us look first at the case $N = 2$. The DOS is

$$\begin{aligned} \rho_{XX}^{(2)}(E) &= \frac{2}{L(L-1)} \sum_{k_1 < k_2} \int_{-\infty}^{+\infty} \frac{d\tau}{2\pi} e^{i\tau[E - J \cos(\frac{2\pi k_1}{L}) - J \cos(\frac{2\pi k_2}{L})]} \\ &= \frac{1}{L(L-1)} \sum_{k_1 \neq k_2} \int_{-\infty}^{+\infty} \frac{d\tau}{2\pi} e^{i\tau[E - J \cos(\frac{2\pi k_1}{L}) - J \cos(\frac{2\pi k_2}{L})]}. \end{aligned} \quad (\text{A17})$$

In order to take the thermodynamic limit for this sum, we need to remove the constraint $k_1 \neq k_2$. To do that, we sum and subtract the terms with $k_1 = k_2$ from the r.h.s. of Eq. (A17). This gives

$$\begin{aligned} \rho_{XX}^{(2)}(E) &= \frac{1}{L(L-1)} \sum_{k_1, k_2} \int_{-\infty}^{+\infty} \frac{d\tau}{2\pi} e^{i\tau[E - J \cos(\frac{2\pi k_1}{L}) - J \cos(\frac{2\pi k_2}{L})]} \\ &\quad - \frac{1}{L(L-1)} \sum_k \int_{-\infty}^{+\infty} \frac{d\tau}{2\pi} e^{i\tau[E - 2J \cos(\frac{2\pi k}{L})]}. \end{aligned} \quad (\text{A18})$$

We can now take the continuum limit, which yields

$$\begin{aligned} \rho_{XX}^{(2)}(E) &= \frac{L}{(L-1)} \int_{-\infty}^{+\infty} \frac{d\tau}{2\pi} \int_{-\pi}^{+\pi} \frac{dq_1}{2\pi} \frac{dq_2}{2\pi} e^{i\tau(E - J \cos q_1 - J \cos q_2)} \\ &\quad - \frac{1}{(L-1)} \int_{-\infty}^{+\infty} \frac{d\tau}{2\pi} \int_{-\pi}^{+\pi} \frac{dq}{2\pi} e^{i\tau(E - 2J \cos q)}. \end{aligned} \quad (\text{A19})$$

Finally, we take the limit $L \rightarrow \infty$. In this limit, the second term on the r.h.s. of Eq. (A19) vanishes, leaving us with the result

$$\rho_{XX}^{(2)}(E) = \int_{-\infty}^{+\infty} \frac{d\tau}{2\pi} e^{i\tau E} \mathcal{J}_0^2(J\tau). \quad (\text{A20})$$

One can repeat this computation for any finite N , which gives

$$\rho_{XX}^{(N)}(E) = \int_{-\infty}^{+\infty} \frac{d\tau}{2\pi} e^{i\tau E} \mathcal{J}_0^N(J\tau). \quad (\text{A21})$$

3. Kurtosis

To compute the kurtosis

$$K(N) = \frac{\langle (E - \langle E \rangle)^4 \rangle}{\langle (E - \langle E \rangle)^2 \rangle^2}, \quad (\text{A22})$$

the first step is to compute the mean energy $\langle E \rangle$,

$$\begin{aligned} \langle E \rangle &= \int_{-NJ}^{NJ} dE E \int_{-\infty}^{\infty} \frac{d\tau}{2\pi} e^{iE\tau} \mathcal{J}_0^N(J\tau) \\ &= 2i \int_{-\infty}^{\infty} \frac{d\tau}{2\pi} \mathcal{J}_0^N(J\tau) \int_0^{NJ} dE E \sin(E\tau) \\ &= 2i \int_{-\infty}^{\infty} \frac{d\tau}{2\pi} \mathcal{J}_0^N(J\tau) \frac{\sin(NJ\tau) - NJ\tau \cos(NJ\tau)}{\tau^2}. \end{aligned} \quad (\text{A23})$$

Since the function \mathcal{J}_0 has even parity, the whole integrand on the r.h.s. of Eq. (A23) has odd parity, and therefore its integral from $-\infty$ to ∞ vanishes. This means that $\langle E \rangle = 0$ for any N , which is a consequence of the fact that the Hamiltonian is symmetric under the transformation $S_z \rightarrow -S_z$. Analogously, any odd moment $\langle E^{2k+1} \rangle$ vanishes as well.

Next, we compute the first two even moments of the energy:

$$\begin{aligned} \langle E^2 \rangle &= \int_{-NJ}^{NJ} dE E^2 \int_{-\infty}^{\infty} \frac{d\tau}{2\pi} e^{iE\tau} \mathcal{J}_0^N(J\tau) \\ &= 2 \int_{-\infty}^{\infty} \frac{d\tau}{2\pi} \mathcal{J}_0^N(J\tau) \int_0^{NJ} dE E^2 \cos(E\tau) \\ &= 2 \int_{-\infty}^{\infty} \frac{d\tau}{2\pi} \mathcal{J}_0^N(J\tau) \frac{2NJ\tau \cos(NJ\tau) + (N^2 J^2 \tau^2 - 2) \sin(NJ\tau)}{\tau^3}, \end{aligned} \quad (\text{A24})$$

and

$$\begin{aligned} \langle E^4 \rangle &= \int_{-NJ}^{NJ} dE E^4 \int_{-\infty}^{\infty} \frac{d\tau}{2\pi} e^{iE\tau} \mathcal{J}_0^N(J\tau) \\ &= 2 \int_{-\infty}^{\infty} \frac{d\tau}{2\pi} \mathcal{J}_0^N(J\tau) \int_0^{NJ} dE E^4 \cos(E\tau) \\ &= 2 \int_{-\infty}^{\infty} \frac{d\tau}{2\pi} \mathcal{J}_0^N(J\tau) \left[\frac{4NJ\tau(N^2 J^2 \tau^2 - 6) \cos(NJ\tau) + (N^4 J^4 \tau^4 - 12N^2 J^2 \tau^2 + 24) \sin(NJ\tau)}{\tau^5} \right]. \end{aligned} \quad (\text{A25})$$

Combining the above two formulae, the expression given in Eq. (7) follows.

-
- [1] Zinner, Nikolaj Thomas, EPJ Web of Conferences **113**, 01002 (2016).
[2] F. Serwane, G. Zürn, T. Lompe, T. B. Ottenstein, A. N. Wenz, and S. Jochim, Science **332**, 336 (2011).
[3] A. N. Wenz, G. Zürn, S. Murmann, I. Brouzos, T. Lompe, and S. Jochim, Science **342**, 457 (2013).
[4] S. Murmann, F. Deuretzbacher, G. Zürn, J. Bjerlin, S. M. Reimann, L. Santos, T. Lompe, and S. Jochim, Phys. Rev. Lett. **115**, 215301 (2015).
[5] S. Murmann, A. Bergschneider, V. M. Klinkhamer, G. Zürn, T. Lompe, and S. Jochim, Phys. Rev. Lett. **114**, 080402 (2015).
[6] K. Jachymski, P. Bienias, and H. P. Büchler, Phys. Rev. Lett. **117**, 053601 (2016).
[7] V. V. Flambaum and F. M. Izrailev, Phys. Rev. E **56**, 5144 (1997).
[8] F. M. Izrailev, Phys. Scr. **T90**, 95 (2001).
[9] C. Ramanathan, P. Cappellaro, L. Viola, and D. G. Cory, New J. Phys. p. 103015 (2011).
[10] I. Bloch, J. Dalibard, and W. Zwerger, Rev. Mod. Phys. **80**, 885 (2008).
[11] P. Jurcevic, B. P. Lanyon, P. Hauke, C. Hempel, P. Zoller, R. Blatt, and C. F. Roos, Nature **511**, 202 (2014).
[12] P. Richerme, Z.-X. Gong, A. Lee, C. Senko, J. Smith, M. Foss-Feig, S. Michalakakis, A. V. Gorshkov, and C. Monroe, Nature **511**, 198 (2014).
[13] T. A. Brody, J. Flores, J. B. French, P. A. Mello, A. Pandey, and S. S. M. Wong, Rev. Mod. Phys. **53**, 385 (1981).
[14] T. Guhr, A. Müller-Groeling, and H. A. Weidenmüller, Phys. Rep. **299**, 189 (1998).
[15] F. Borgonovi, F. M. Izrailev, L. F. Santos, and V. G. Zelevinsky, Phys. Rep. **626**, 1 (2016).
[16] L. F. Santos, F. Borgonovi, and F. M. Izrailev, Phys. Rev. Lett. **108**, 094102 (2012).
[17] L. F. Santos, F. Borgonovi, and F. M. Izrailev, Phys. Rev. E **85**, 036209 (2012).
[18] J. A. Kjäll, J. H. Bardarson, and F. Pollmann, Phys. Rev. Lett. **113**, 107204 (2014).
[19] E. J. Torres-Herrera and L. F. Santos, Ann. Phys. (Berlin) **529**, 1600284 (2017), ISSN 1521-3889.
[20] V. V. Flambaum and F. M. Izrailev, Phys. Rev. E **64**, 036220 (2001).
[21] E. J. Torres-Herrera and L. F. Santos, Phil. Trans. R. Soc. A **375**, 20160434 (2017).
[22] E. J. Torres-Herrera, A. García-García, and L. F. Santos, arXiv:1704.06272.
[23] M. Akila, D. Waltner, B. Gutkin, P. Braun, and T. Guhr, Phys. Rev. Lett. **118**, 164101 (2017).
[24] L. Fleishman and P. W. Anderson, Phys. Rev. B **21**, 2366 (1980).
[25] D. L. Shepelyansky, Phys. Rev. Lett. **73**, 2707 (1994).
[26] L. F. Santos and M. I. Dykman, Phys. Rev. B **68**, 214410 (2003).
[27] L. F. Santos and M. I. Dykman, New J. Phys. **14**, 095019 (2012).
[28] L. F. Santos, J. Math. Phys. **50**, 095211 (2009).
[29] J. B. French and S. S. M. Wong, Phys. Lett. B **33**, 449 (1970).
[30] M. Takahashi, *Thermodynamics of One-Dimensional Solvable Models* (Cambridge University Press, 2005), 2nd ed., ISBN 0521019796.
[31] M. L. Mehta, *Random Matrices* (Academic Press, Boston, 1991).
[32] E. J. Torres-Herrera, M. Vyas, and L. F. Santos, New J. Phys. **16**, 063010 (2014).

- [33] E. J. Torres-Herrera and L. F. Santos, *Phys. Rev. E* **89**, 062110 (2014).
- [34] S. Trotzky, P. Cheinet, S. Fölling, M. Feld, U. Schnorrberger, A. M. Rey, A. Polkovnikov, E. A. Demler, M. D. Lukin, and I. Bloch, *Science* **319**, 295 (2008).
- [35] M. Schreiber, S. S. Hodgman, P. Bordia, H. P. Lüschen, M. H. Fischer, R. Vosk, E. Altman, U. Schneider, and I. Bloch, *Science* **349**, 842 (2015).
- [36] E. J. Torres-Herrera, J. Karp, M. Távora, and L. F. Santos, *Entropy* **18**, 359 (2016).
- [37] M. Távora, E. J. Torres-Herrera, and L. F. Santos, *Phys. Rev. A* **94**, 041603 (2016).
- [38] M. Távora, E. J. Torres-Herrera, and L. F. Santos, *Phys. Rev. A* **95**, 013604 (2017).
- [39] T. Devakul and R. R. P. Singh, *Phys. Rev. Lett.* **115**, 187201 (2015).
- [40] W. De Roeck, F. Huveneers, M. Müller, and M. Schiulaz, *Phys. Rev. B* **93**, 014203 (2016).
- [41] F. C. Alcaraz, M. N. Barber, M. T. Batchelor, R. J. Baxter, and G. R. W. Quispel, *J. Phys. A* **20**, 6397 (1987).
- [42] F. C. Alcaraz, M. N. Barber, and M. T. Batchelor, *Ann. Phys.* **182**, 280 (1988).
- [43] L. F. Santos, M. Távora, and F. Pérez-Bernal, *Phys. Rev. A* **94**, 012113 (2016).